Published in final edited form as:
ACS Chem Neurosci. 2024 June 19; 15(12): 2396–2407. doi:10.1021/acschemneuro.4c00086.

Computer-Aided Design and Biological Evaluation of Diazaspirocyclic D_4R Antagonists

Caleb A. H. Jones[¶],
Warren Center for Neuroscience Drug Discovery and Department of Pharmacology, Vanderbilt University School of Medicine, Nashville, Tennessee 37232, United States; Department of Chemistry, Vanderbilt University, Nashville, Tennessee 37232, United States;

Benjamin P. Brown[¶],
Department of Chemistry, Center for Structural Biology, and Center for Applied AI in Protein Dynamics, Vanderbilt University, Nashville, Tennessee 37232, United States

Daniel C. Schultz[¶],
Warren Center for Neuroscience Drug Discovery and Department of Pharmacology, Vanderbilt University School of Medicine, Nashville, Tennessee 37232, United States; Department of Chemistry, Vanderbilt University, Nashville, Tennessee 37232, United States

Julie Engers,
Warren Center for Neuroscience Drug Discovery and Department of Pharmacology, Vanderbilt University School of Medicine, Nashville, Tennessee 37232, United States; Department of Chemistry, Vanderbilt University, Nashville, Tennessee 37232, United States

Valerie M. Kramlinger,
Warren Center for Neuroscience Drug Discovery and Department of Pharmacology, Vanderbilt University School of Medicine, Nashville, Tennessee 37232, United States; Department of Chemistry, Vanderbilt University, Nashville, Tennessee 37232, United States

Jens Meiler,

Corresponding Authors: Craig W. Lindsley – *Warren Center for Neuroscience Drug Discovery and Department of Pharmacology, Vanderbilt University School of Medicine, Nashville, Tennessee 37232, United States; Department of Chemistry, Vanderbilt University, Nashville, Tennessee 37232, United States;* craig.lindsley@vanderbilt.edu, Jens Meiler – *Department of Chemistry, Center for Structural Biology, and Center for Applied AI in Protein Dynamics, Vanderbilt University, Nashville, Tennessee 37232, United States; Institute for Drug Discovery, Leipzig University Medical School, Leipzig SAC 04103, Germany*; jens.meiler@vanderbilt.edu, Caleb A. H. Jones – *Warren Center for Neuroscience Drug Discovery and Department of Pharmacology, Vanderbilt University School of Medicine, Nashville, Tennessee 37232, United States; Department of Chemistry, Vanderbilt University, Nashville, Tennessee 37232, United States;* caleb.a.jones@vanderbilt.edu.

[¶]C.A.H.J., B.P.B., and D.C.S. contributed equally to this work and are listed as co-first authors. C.A.H.J. and D.C.S. contributed to the synthesis and characterization of all the compounds. B.P.B. contributed through the modeling of the various D_4R antagonists in silico. J.E. organized the samples shipment to Eurofins and worked up the data for percent inhibition, K_i and IC_{50}. V.M.K. contributed by the design and experimentation of DMPK evaluation. J.M. and C.W.L. conceived the study and contributed as project leads.

Supporting Information
The Supporting Information is available free of charge at https://pubs.acs.org/doi/10.1021/acschemneuro.4c00086.
Experimental procedure for the synthesis of compounds, ^{1}H and ^{13}C{^{1}H} NMR spectra for all compounds, 2D NMR (NOESY, HMBC, HSQC, and COSY) for compounds that required further characterization, DMPK experimental methods, computational methods, and metabolite profiling (PDF)

Notes
The authors declare no competing financial interest.

Complete contact information is available at: https://pubs.acs.org/10.1021/acschemneuro.4c00086

Department of Chemistry, Center for Structural Biology, and Center for Applied AI in Protein Dynamics, Vanderbilt University, Nashville, Tennessee 37232, United States; Institute for Drug Discovery, Leipzig University Medical School, Leipzig SAC 04103, Germany;

Craig W. Lindsley

Warren Center for Neuroscience Drug Discovery and Department of Pharmacology, Vanderbilt University School of Medicine, Nashville, Tennessee 37232, United States; Department of Chemistry, Vanderbilt University, Nashville, Tennessee 37232, United States;

Abstract

Parkinson's disease (PD) is a neurodegenerative disorder characterized by the progressive loss of dopaminergic neurons in the substantia nigra, resulting in motor dysfunction. Current treatments are primarily centered around enhancing dopamine signaling or providing dopamine replacement therapy and face limitations such as reduced efficacy over time and adverse side effects. To address these challenges, we identified selective dopamine receptor subtype 4 (D_4R) antagonists not previously reported as potential adjuvants for PD management. In this study, a library screening and artificial neural network quantitative structure–activity relationship (QSAR) modeling with experimentally driven library design resulted in a class of spirocyclic compounds to identify candidate D_4R antagonists. However, developing selective D_4R antagonists suitable for clinical translation remains a challenge.

Graphical Abstract

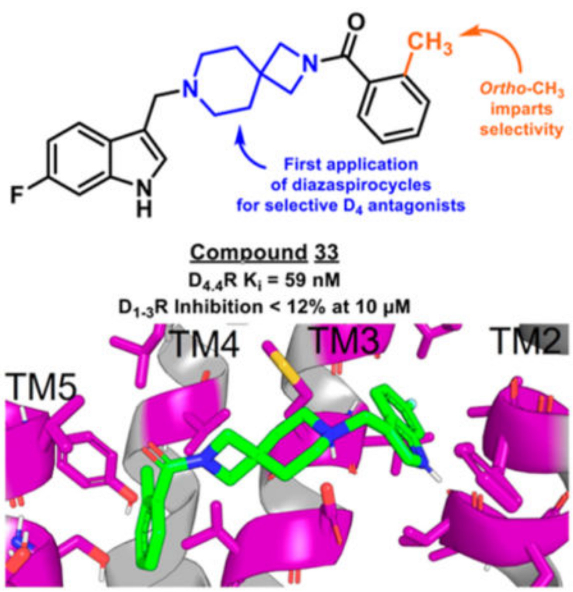

Keywords

dopamine receptors; D_4R antagonism; Parkinson's disease

INTRODUCTION

Parkinson's disease (PD) is a debilitating neurodegenerative disorder characterized by progressive motor dysfunction resulting from the degeneration of dopaminergic neurons in the substantia nigra.[1,2] The resulting dopamine deficiency leads to the classic motor symptoms of PD, including bradykinesia, resting tremors, and rigidity.[1] While current treatments, such as enhancing dopamine signaling and providing dopamine replacement therapy, have been effective in alleviating motor symptoms in the early stages of PD, the need for innovative therapeutic approaches is underscored by the challenges of maintaining their long-term efficacy and minimizing the risk of side effects, including medication-induced dyskinesias.[2,3] One promising avenue of exploration lies in the design and development of selective dopamine receptor subtype 4 (D_4R) antagonists as potential adjuvants for PD management.[4–6]

Dopamine receptors are divided into two families based on structural similarities, function, and pharmacological properties: the D_1-like receptor family, which includes primarily the D_1R and D_5R subtypes, and the D_2-like receptor family, which includes D_2R, D_3R, and D_4R.[7–9] Functionally, these two families have opposing mechanisms, with D_1-like receptors stimulating adenyl cyclase through $G_{\alpha s}$ signaling and D_2-like receptors inhibiting adenyl cyclase through $G_{\alpha i/o}$ signaling.[7] Further receptor subtype heterogeneity can be found at the level of genetic polymorphisms. D_4R itself comprises 10 different genotypes, with $D_{4.2}$, $D_{4.4}$, and $D_{4.7}$ being the most prevalent of these.[10–12] The pharmacological management of PD currently focuses primarily on enhancing dopamine signaling through D_2R, such as by providing dopamine precursor therapy with levodopa or through direct agonism with pramipexole or ropinirole.[13–25]

D_4R has garnered increasing attention in recent years due to its distinctive expression pattern within the central nervous system and its potential role in modulating dopamine signaling.[5,6,26] Unlike other dopamine receptor subtypes, D_4R is primarily located in the frontal cortex and limbic system, areas that are associated with cognitive and emotional processes, and consequently has been implicated largely in neuropsychiatric conditions (though D_4R is also expressed in the periphery).[27–40] Early D_4R antagonists were considered as potential therapeutic avenues for diseases such as addiction and attention-deficit/hyperactivity disorder (ADHD).[41–44] Additionally, due to the expression of D_4R within the basal ganglia, which is associated with the development of dyskinesias in PD patients, research has also unveiled the involvement of D_4R in motor control, making it a compelling target in the context of PD for the treatment of levodopa-induced dyskinesia (LID).[3,4,33,45–48] Consequentially, interest in the development of selective D_4R antagonists has increased in recent decades, selected examples of which can be seen in Figure 1. The approved antipsychotics clozapine and haloperidol have also been included for reference due to their historical significance, though these are not selective for D_{4R}.[9,30,49–59]

The central challenge in designing D_4R antagonists as an adjuvant therapy for PD lies in obtaining selectivity for D_4R over the other dopamine receptor subtypes, action at which could produce undesired side effects. For instance, antagonism or partial agonism of D_2R has been demonstrated to worsen Parkinsonism, while action at D_1R in conjunction with levodopa administration is associated with increased LID severity.[60–64] Therefore, the pursuit of D_4R antagonists for PD therapy demands meticulous attention to the selectivity and efficacy of the designed compounds. Recent advances in synthetic chemistry, structural biology, and pharmacology have enabled the design and characterization of diverse selective D_4R antagonists, as exemplified in several key studies.[59,65–69] Building off of these rich structure–activity relationship data, we disclose herein the development of a novel class of potent, selective D_4R antagonists suitable for further preclinical optimization.

RESULTS

Ligand-Based Ultralarge Library Screening to Identify Candidate D_4R Antagonists.

To identify new D_4R antagonists, we first performed ligand-based ultralarge library screening using multitask classification artificial neural network (ANN) quantitative structure–activity relationship (QSAR) models (see Computational Methods and Materials in the Supporting Information). We trained four unique QSAR models on publicly available confirmatory screening data (molecules had reported IC_{50} and/or K_i/K_d values) from PubChem, one each for D_2R, D_3R, D_4R, and D_5R. Each model was trained to predict the likelihood that a molecule is active at or below the following thresholds: 1, 10, 100, 1000, and 10,000 nM. Two primary metrics guided our analysis: (1) the probability that a molecule is active against D_4R at or below 10 nM and (2) the predicted selectivity for D_4R, where selectivity is given by the equation below.

$$\text{Selectivity} = \frac{P_{\text{D}_4\text{R, 10nM}}}{P_{\text{D}_4\text{R, 10nM}} + P_{\text{D}_2\text{R, 1000nM}} + P_{\text{D}_3\text{R, 1000nM}} + P_{\text{D}_5\text{R, 1000nM}}}$$

where $P_{\text{D}_4\text{R, 10nM}}$ is the QSAR-predicted probability of a molecule to be active at or below 10 nM, $P_{\text{D}_4\text{R, 1000nM}}$ is the same metric for D_2R at or below 1000 nM, etc. Our formulation of selectivity specifically evaluates the likelihood of a molecule being selective for D_4R at 2 orders of magnitude (active at 10 nM D_4R vs 1000 nM D_2, D_3, and D_5).

We applied our QSAR models to screen over 1 billion molecules sourced from LifeChemicals and the Enamine REAL database (Figure 2A). Compounds with 10 nM D_4R activity prediction scores at or above 0.8 were moved forward for further analysis. Preference was given to compounds also exhibiting a selectivity score exceeding 0.4. We performed property-based flexible alignment[70] of a subset of 500 molecules to the crystallographically bound pose of the D_4R-selective antagonist L-745,870,[68] followed by visual inspection. Ultimately, we chose 89 molecules to acquire from Enamine and LifeChemicals for experimental screening at Eurofins Discovery.

Our screening efforts yielded notable outcomes, with 38 of the selected molecules displaying inhibitory activity exceeding 50% at 10 μM and 17 (see Supporting Information for structures) showing greater than 85% inhibition at 10 μM for D_4R (Figure 2B,C). Our success for identifying selective molecules was much lower. This is not unexpected as the selectivity metric is built from multiple independent predictions (eq S1), and thus, error from each prediction accumulates in the final score. Frequently, molecules predicted to be D_4R

selective were only selective against a single off-target subtype. Nonetheless, a subset of D_4R-active compounds exhibited varying degrees of selectivity relative to at least one other dopamine receptor subtype (Figure 2B).

Identification of a Spirocyclic Core for D_4R Antagonists.

From our initial screen, we identified compound *VU6052469*, which is structurally similar to a previously published D_4R antagonist by Carato et al. bearing a piperidine core with a naphthamide substituent that exhibits high potency and selectivity for D_4R over D_2R;[71] however, *VU6052469* itself is nonselective (Figure 2B,D). We docked *VU6052469* and the Carato compound into D_4R (PDB ID: 6IQL)[68] to investigate the potential binding mode of our hit (Figure 2E). One challenge with designing D_4R antagonists is the topological pseudosymmetry of D_4R-active compounds, which in the case of *VU6052469* and the Carato compound entails two distal aryl rings linked to a piperidine core (Figure 2D). In principle, this symmetry could enable the molecules to bind such that the halogen-substituted phenyl ring interacts with either transmembrane helices 2 (TM2) and TM3 (Figure S103A) or alternatively with TM4/5/6 (Figure S103B). In either binding pose, for example, *VU6052469* hydrogen bonds with the conserved D3.32 side chain, and V3.33 can stack with its aromatic rings (Figure S103). The pocket formed by TM2/3 is hydrophobic and has previously been implicated in ligand selectivity.[68,69] Indeed, the TM2/3 interface differs between D_4R and D_2R in that D_2R contains aromatic ring side chains, while in D_4R, there are aliphatic chains (Figure S104). In contrast, the amino acid composition of TM4/5/6 is a mixture of polar and hydrophobic residues. Notably, a cluster of serine residues engaged in internal backbone hydrogen bonds in TM5/6 renders this portion of the pocket more sterically accessible.

We reasoned that the latter pose is less likely as it induces a greater loss of planarity of the amide linker within the docked pose, which is supported by density functional theory (DFT) conformational stability calculations and molecular orbital analysis performed at the wB97X-D/6–311G(d,p) level of theory[72] (Figure S103C,D). We estimate that the first pose of *VU6052469* (Figure S103A) is 11.3 kcal/mol more energetically favorable, and it follows that the Carato compound adopts a similar binding conformation (Figure 2E). Despite being nonselective, our docked poses suggest that *VU6052469* could readily be made selective through extending the amide bond via a methylene linker and truncating the arene without altering the orientation of the ligand within the binding pocket. To that end, we replaced the secondary amide with an azetidine amide to give a 2,7-diazaspiro[3.5]nonane core, resulting in compound **4**, which displayed selectivity for D_4R with only a partial loss of on-target activity (Table 1).

To better understand the mechanism of selectivity imparted by the spirocyclic core, we docked **4** into D_4R and D_2R (see Supporting Information) (Figure 3A–C). We verified the binding mode by running molecular dynamics (MD) simulations and analyzing ligand root-mean-square-deviation (rmsd) over time (Figure S105). Our docked poses suggest that the difluorophenyl of **4** differentially engages the TM2/3 hydrophobic pocket in D_4R versus D_2R. Compared to its complex with D_4R, in the D_2R complex **4** is shifted deeper into the TM2/3 pocket such that the hydrogen bond geometry between the orthosteric pocket aspartate D3.32 and the protonated piperidine is suboptimal (Figure S106). We confirmed that the D_2R electrostatic interactions are less favorable than D_4R by performing geometry optimization and subsequent interface energy calculations of the complexes using the semiempirical quantum mechanics (QM) tightbinding density functional theory (DFTB) method with dispersion corrections, DFTB3-D3(BJ) (Figure 3D) (see Supporting Information).[73,74] The interaction energies of **4** with respect to the conserved central aspartate D3.32 and TM2/3 hydrophobic pocket in D_4R and D_2R are estimated to be −24.46 and −18.53 kcal/mol, respectively (Figure 3D).

Optimization of Spirocyclic D_4R Antagonist Potency and Selectivity.

We sought to improve upon the potency and selectivity of **4** by screening analogues with differing polar aromatic or heteroaromatic groups on the southern end of the compound, installing methyl groups at the 2 or 3 position of the piperidine and probing the effect of the substitution pattern and substituent type on the northern phenyl ring on activity (Tables 1 and 2). The general synthetic scheme for this class of compounds is shown in Scheme 1, and detailed experimental procedures are provided in the Supporting Information for all intermediates and final compounds as well as compound **1.** Briefly, compound **1** underwent TFA-mediated *boc*-deprotection followed by HATU amide coupling to afford intermediate **2.** Subsequent benzyloxycarbonyl removal via hydrogen over palladium reduction gave key intermediate **3,** which was subjected to either reductive amination with assorted aryl aldehydes to afford compounds **5–12** or an S_N2 reaction with 3,4-difluorobenzyl bromide to provide compound **4.** To obtain azetidine amides **17–33,** commercially available *tert*-butyl 2,7-diazaspiro[3.5]nonane-2-carboxylate was subjected to reductive amination with 6-fluoro-1*H*-indole-3-carbaldehyde to give intermediate **15.** *Boc*-deprotection with TFA afforded **16,** which then underwent HATU amide coupling with assorted aryl carboxylic acids to give compounds **17–34.**

Overall, this focused collection of spirocyclic antagonists provided a number of valuable SAR insights. With respect to the southern region, replacing the difluorophenyl moiety with the analogous dichlorophenyl substituent (**9**) resulted in significantly increased activity; however, a significant decrease in selectivity between the DR subtypes was also observed. Incorporation of other substituted arenes, such as fluorophenol (**8**), benzodioxole (**11**), and fluoropyridine (**10**), resulted in a steep decrease in inhibition (Table 1). By installing a 6-fluoroindole heterocycle (**5**) as we used previously in our morpholine core D_4R antagonist (VU6004432, Figure 1),[58] we observed drastically improved activity over **4,** though the overall selectivity was mildly decreased. Exchanging the indole for an indazole **6** resulted in an improvement in the selectivity against all subtypes, with a mild improvement in activity at $D_{4.4}R$. This is in stark contrast to the incorporation of benzisoxazole (**7**), which essentially abolishes activity. Modifications to the spirocyclic core were not favorable as the addition of methyl groups to the 2 or 3 position of the piperidine ring (compounds **14** and **13,** respectively) significantly reduced the potency and affinity of the compound compared to that observed with **5** (Table 1);, while expansion of the azetidine to a pyrrolidine led to a substantial decrease in inhibitory activity (compound **42;** see Supporting Information).

To better understand the differences in activity between **5, 6,** and **7,** we first docked **5** to D_4R. Once again, pseudosymmetry within **5** rendered two flipped binding modes plausible. The first binding mode (Figure 3E) follows from the predicted poses of *VU6052469* and **4.** Interestingly, however, an alternative binding mode in which the indole ring of **5** adopts a pose mimicking the experimentally determined bound pose of L745,870[68] is also possible. To determine which pose is more likely, we performed MD simulations starting from each docked pose. We observed that the pose consistent with **4** (Figure 3E) is more likely to remain near the docked binding pose (Figure S107A,B) and adopt favorable hydrogen bond geometry with D3.32 (Figure S107C,D). Furthermore, the interaction energy rankings for this binding mode (Figure 3E) are consistent with the experimental results and demonstrate the activity cliff in **7** (Table 1 and Figure 4A,B). In contrast, the binding mode mimicking the L745,870 pose yields interaction energy estimates inconsistent with experiment (data not shown). Visualization of the surface electrostatic potentials of D_4R complexed with **5, 6,** or **7** at the DFT wB97X-D/6–31G(d) level of theory[72] suggests that this activity cliff is due to loss of complementary electrostatic interactions and an abundance of anionic charge near TM2 (Figure 4C–E).

While indazole antagonist **6** provided the best potency and selectivity profile thus far, we proceeded with the combination of the 6-fluoroindole southern ring and the unmodified 2,7-diazaspiro[3.5]nonane core for exploration of the northern region SAR as **5** performed similarly and was more costeffective for library synthesis. Therefore, we employed **5** as a starting point for pursuing a focused library of aryl amides on the northern end of the scaffold for further improvement of DR subtype selectivity (Table 2). Overall, alkyl and chloro substituents were well-tolerated, with the sole exception of the 3,5-dichlorophenyl analogue (**28**), which demonstrated drastically reduced inhibitory activity (49%). The 2,4-dichlorophenyl regioisomer (**19**) retained activity, however, indicating that $D_{4.4}R$ inhibition is sensitive to subtle changes in substitution pattern in this region. In contrast to alkyl and chloro groups, incorporation of alkoxy groups generally led to a significant reduction in activity against $D_{4.4}R$ (**23–26**), with the sole exception being **20** (Figure 3F), which bears a benzodioxole heterocycle ($D_{4.4}R$ IC_{50} = 84 nM; K_i = 23 nM). The potency of benzodioxole-bearing compound **20** suggests that the lack of activity observed in compounds **23–26** is a result of unfavorable steric interactions facilitated by their freely rotating alkyl groups rather than ring electronics. In addition to the benzodioxole example (**20**), increasing the size of the aryl amide from a monocycle to a fused bicycle in other instances was also well tolerated (**27, 31**), with naphthalene **27** exhibiting particularly potent activity ($D_{4.4}R$ IC_{50} = 28 nM; K_i = 7.6 nM). With respect to selectivity, a strong sensitivity to regioisomerism was observed, which was most clearly demonstrated in compounds **29, 32,** and **33,** which bear *para*-, *meta*-, and *ortho*-toluamides, respectively. Of these, compound **29** demonstrates the highest $D_{4.4}R$ activity ($D_{4.4}R$ IC_{50} = 62 nM; K_i = 17 nM), and it exhibits a moderately improved selectivity profile over **5.** Both *meta* and *ortho* isomers (compounds **32** and **33,** respectively) display reduced activity compared to *para* isomer **29.** Compound **33** (Figure 3G), however, exhibited the best selectivity profile of all compounds disclosed herein, with a notable 0% activity against D_{2S}. It was also observed that replacement of the *para*-toluamide of **29** with a tosylamide (**34**) mildly reduced the $D_{4.4}R$ activity but notably increased the inhibitory activity at all other tested DR subtypes, possibly due to the reduced planarity of the sulfonamide.

In Vitro and In Vivo DMPK Analysis of Selected Compounds.

A subset of compounds that demonstrated high potency and excellent selectivity were selected for pharmacokinetic characterization (Table 3). In vitro stability experiments in rat and human microsomes returned high clearance (>70% Q_h) across all compounds, except for **20,** which exhibited moderate hepatic clearance (CL_H of 13.7 and 36.2 in human and rat microsomes, respectively). The free fraction in plasma ranged from 1 to 19% in rat and 3–26% in human. Notably, both compounds **33** and **20** exhibited increased free fractions compared to the original hit (**4**). Three compounds (**4, 20,** and **33**) were selected to assess in vivo pharmacokinetics (compounds **29** and **32** were excluded as they exhibited worse free fraction in plasma compared to **20** and **33**). Upon intravenous dosing in rats, all three compounds demonstrated superhepatic clearance (>100% Q_h). This result is consistent with these compounds experiencing high hepatic metabolic clearance and may also indicate contribution to clearance through a different route, such as extrahepatic metabolism or active direct excretion. Despite high clearance, compounds **4, 20,** and **33** exhibited moderate to high distribution into tissues (volume of distributions of 5.52, 44.4, and 36.9 L/kg, respectively), explaining the reasonable half-lives for these compounds (1.05, 4.55, and 4.02 h, respectively).

Compound **33** was subjected to metabolite profiling in human and rat hepatocytes to provide insight into potential clearance mechanisms and metabolic liabilities (Figure 5). After incubation for 4 h, **33** exhibited low turnover in human hepatocytes and moderate turnover in rat hepatocytes, with 87.9 and 65.8% of parent compound (**33**) remaining postincubation, respectively. In both species, only two major metabolites were observed: mono-oxidation of the benzylic methyl group and piperidine *N*-dealkylation. The latter means of metabolism was elevated in rats (32.4%) compared to that in humans (6.3%).

DISCUSSION

The application of spirocycles to drug discovery efforts has increased in recent years as a means to increase compound three-dimensionality, modulate DMPK properties, incorporate additional sp^3 centers, and generate novel intellectual property.[75–78] One of the central findings of the present study was the discovery of 2,7-diazaspiro[3.5]nonane as an applicable core motif for selective D_4R antagonists. While we initially identified the highly potent antagonist *VU6052469*, which exhibited a high degree of structural similarity to a previously reported selective D_4R antagonist,[71] it notably lacked selectivity (Figure 2B,D,E). We postulated that this lack of selectivity arose from the difference in length between these two compounds, with the naphthalene and 4-chlorobenzyl moieties of the Carato compound potentially leading to poorer steric interactions within the TM2/3 pocket of D_2R than the dimethylphenyl and 3,4-difluorobenzyl moieties of *VU6052469* (Figure 2E). By replacing the core piperidine of *VU6052469* with 2,7-diazaspiro[3.5]nonane, the dimethylphenyl ring is extended further into the TM4/5/6 pocket, affording potent and selective activity against D_4R (Table 1). While there have been reported examples of substituted diazaspirocycles bearing D_4R activity, this activity was not the desired mode of action (i.e., the intent was to target σ receptors) nor did the more potent compounds exhibit DR subtype selectivity.[79] Therefore, to the best of our knowledge, this is the first report of the use of diazaspirocycles in pursuit of selective D_4R antagonists.

Interestingly, our investigation revealed an activity cliff when comparing the indole/indazole- vs benzisoxazole-substituted compounds (compounds **5/6** and **7,** respectively). Activity cliffs are subtle structural changes leading to significant alterations in inhibitory activity. In this case, the subtle difference in ligand interaction energies with the receptor went undetected by the docking score function. It was only after performing geometry optimization and interaction energy calculations with the more computationally demanding semiempirical QM method DFTB3-D3(BJ) that we understood the case of the reduction in binding affinity, which was a result of an accumulation of anionic charge near TM2 with no available hydrogen bond donors. This example emphasizes the continued importance of developing force fields and/or deep learning algorithms for binding affinity prediction that can be used during rapid screening protocols.

A key challenge in the rational design of selective D_4R antagonists is the topological pseudosymmetry displayed by most antagonists. This challenge is 2-fold: (1) highly similar antagonists may be oriented in conformations 180° opposed to one another, and (2) the internal pseudosymmetry of many D_4R antagonists renders it difficult to ascertain their appropriate binding modes. Despite extensive computational validation, it is possible that our putative binding modes are inaccurate, which may lead to false structure–activity relationships. Further experimental structural evidence, such as crystal structures of these spirocyclic antagonists bound to D_4R, will be valuable in the design of future D_4R antagonists with similar potencies and selectivity.

Modifications to the northern aryl amide of this scaffold demonstrated the sensitivity of D_4R potency and selectivity to ring substituent choice and regioisomerism. Overall, compound **33,** which bears an *ortho*-toluamide northern substituent, displayed the best selectivity profile of the tested compounds while retaining potent $D_{4.4}R$ antagonism and affinity (IC_{50} = 210 nM; K_i = 59 nM). Though our study has yielded promising D_4R antagonists such as this, an ongoing challenge in the design of this class of compounds is the optimization of pharmacokinetic properties. While this class of compounds exhibited excellent aqueous solubility (see Supporting Information), both in vitro and in vivo pharmacokinetic analysis of selected compounds demonstrated a key limitation of the present class: high metabolic clearance. The findings of these assays underscore the need for continued efforts to improve the pharmacokinetic profiles of potential D_4R antagonist drug candidates, most likely via design changes to remove metabolic hotspots within this chemical series.

Altogether, our study has unveiled a spirocyclic core for D_4R selective antagonists, providing a foundation for further drug development efforts in the context of PD. Our insight into DR subtype selectivity and activity cliffs offers valuable guidance for future research in this area. The improvement of spirocyclic D_4R antagonist DMPK properties, however, remains requisite for the development of a suitable preclinical lead within this class as a potential adjuvant therapy for PD.

Supplementary Material

Refer to Web version on PubMed Central for supplementary material.

ACKNOWLEDGMENTS

B.P.B. is supported by the National Institutes of Health's National Institute on Drug Abuse (NIH NIDA DP1DA058349). J.M. is supported by a Humboldt Professorship of the Alexander von Humboldt Foundation, and research in the Meiler Lab at Vanderbilt University is supported by the NIH (NIDA R01DA046138, NLM R01LM013434, NCI R01CA227833, and NIGMS R01GM080403). J.M. acknowledges funding by the Deutsche Forschungsgemeinschaft (DFG) through SFB1423 (421152132). J.M. is supported by BMBF (Federal Ministry of Education and Research) through the Center for Scalable Data Analytics and Artificial Intelligence (ScaDS.AI). This work is partly supported by BMBF (Federal Ministry of Education and Research) through DAAD project 57616814 (SECAI, School of Embedded Composite AI). High-performance computing at Vanderbilt's ACCRE facility is supported through NIH S10 OD016216, NIH S10 OD020154, and NIH S10 OD032234. Authors would also thank the William K. Warren Family and Foundation for founding the William K. Warren Jr. Chair in Medicine and endowing the WCNDD and support of our programs. We would like to thank Jeremy Turkett for performing the metabolite profiling of compound **33** and Christopher Presley for performing the kinetic solubility assays.

REFERENCES

(1). Gelb DJ; Oliver E; Gilman S Diagnostic Criteria for Parkinson Disease. Arch. Neurol 1999, 56 (1), 33. [PubMed: 9923759]

(2). Lee TK; Yankee EL A Review on Parkinson's Disease Treatment. Neuroimmunol. Neuroinflammation 2022, 8, 222.

(3). Huot P; Johnston TH; Koprich JB; Fox SH; Brotchie JM The Pharmacology of L-DOPA-Induced Dyskinesia in Parkinson's Disease. Pharmacol. Rev 2013, 65 (1), 171–222. [PubMed: 23319549]

(4). Sebastianutto I; Maslava N; Hopkins CR; Cenci MA Validation of an Improved Scale for Rating L-DOPA-Induced Dyskinesia in the Mouse and Effects of Specific Dopamine Receptor Antagonists. Neurobiol. Dis 2016, 96, 156–170. [PubMed: 27597526]

(5). Lindsley CW; Hopkins CR Return of D_4 Dopamine Receptor Antagonists in Drug Discovery: Miniperspective. J. Med. Chem 2017, 60 (17), 7233–7243. [PubMed: 28489950]

(6). Giorgioni G; Del Bello F; Pavletić P; Quaglia W; Botticelli L; Cifani C; Micioni Di Bonaventura E; Micioni Di Bonaventura MV; Piergentili A Recent Findings Leading to the Discovery of Selective Dopamine D4 Receptor Ligands for the Treatment of Widespread Diseases. Eur. J. Med. Chem 2021, 212, 113141. [PubMed: 33422983]

(7). Kebabian JW Multiple Classes of Dopamine Receptors in Mammalian Central Nervous System: The Involvement of DopamineSensitive Adenylyl Cyclase. Life Sci 1978, 23 (5), 479–483. [PubMed: 357876]

(8). Missale C; Nash SR; Robinson SW; Jaber M; Caron MG Dopamine Receptors: From Structure to Function. Physiol. Rev 1998, 78 (1), 189–225. [PubMed: 9457173]

(9). Vallone D; Picetti R; Borrelli E Structure and Function of Dopamine Receptors. Neurosci. Biobehav. Rev 2000, 24 (1), 125–132. [PubMed: 10654668]

(10). Tol HHMV; Wu CM; Guan H-C; Ohara K; Bunzow JR; Civelli O; Kennedy J; Seeman P; Niznik HB; Jovanovic V Multiple Dopamine D4 Receptor Variants in the Human Population. Nature 1992, 358 (6382), 149–152. [PubMed: 1319557]

(11). Chang F-M; Kidd JR; Livak KJ; Pakstis AJ; Kidd KK The World-Wide Distribution of Allele Frequencies at the Human Dopamine D4 Receptor Locus. Hum. Genet 1996, 98 (1), 91–101. [PubMed: 8682515]

(12). Ding Y-C; Chi H-C; Grady DL; Morishima A; Kidd JR; Kidd KK; Flodman P; Spence MA; Schuck S; Swanson JM; Zhang Y-P; Moyzis RK Evidence of Positive Selection Acting at the Human Dopamine Receptor D4 Gene Locus. Proc. Natl. Acad. Sci. U.S.A 2002, 99 (1), 309–314. [PubMed: 11756666]

(13). Schneider CS; Mierau J Dopamine Autoreceptor Agonists: Resolution and Pharmacological Activity of 2,6-Diaminotetrahydro-benzothiazole and an Aminothiazole Analog of Apomorphine. J. Med. Chem 1987, 30 (3), 494–498. [PubMed: 3820220]

(14). Mierau J; Schingnitz G Biochemical and Pharmacological Studies on Pramipexole, a Potent and Selective Dopamine D2 Receptor Agonist. Eur. J. Pharmacol 1992, 215 (2–3), 161–170. [PubMed: 1356788]

(15). Mierau J; Schneider FJ; Ensinger HA; Chio CL; Lajiness ME; Huff RM Pramipexole Binding and Activation of Cloned and Expressed Dopamine D2, D3 and D4 Receptors. Eur. J. Pharmacol., Mol. Pharmacol. Sect 1995, 290 (1), 29–36.

(16). Bennett JP; Piercey MF Pramipexole a New Dopamine Agonist for the Treatment of Parkinson’s Disease. J. Neurol. Sci 1999, 163 (1), 25–31. [PubMed: 10223406]

(17). Antonini A; Barone P; Ceravolo R; Fabbrini G; Tinazzi M; Abbruzzese G Role of Pramipexole in the Management of Parkinson’s Disease: CNS Drugs 2010, 24 (10), 829–841. [PubMed: 20839895]

(18). Frampton JE Pramipexole Extended-Release: A Review of Its Use in Patients with Parkinson’s Disease. Drugs 2014, 74 (18), 2175–2190. [PubMed: 25385556]

(19). Gallagher G; Lavanchy PG; Wilson JW; Hieble JP; DeMarinis RM 4-[2-(Di-n-Propylamino)Ethyl]-2(3H)-Indolone: A Prejunctional Dopamine Receptor Agonist. J. Med. Chem 1985, 28 (10), 1533–1536. [PubMed: 4045928]

(20). Eden RJ; Costall B; Domeney AM; Gerrard PA; Harvey CA; Kelly ME; Naylor RJ; Owen DAA; Wright A Preclinical Pharmacology of Ropinirole (SK&F 101468-A) a Novel Dopamine D2 Agonist. Pharmacol., Biochem. Behav 1991, 38 (1), 147–154. [PubMed: 1673248]

(21). Stacy M Update on ropinirole in the treatment of Parkinson’s disease. Neuropsychiatr. Dis. Treat 2008, 33, 33.

(22). Funk C LXV.Synthesis of Dl-3:4-Dihydroxyphenylalanine. J. Chem. Soc., Trans 1911, 99 (0), 554–557.

(23). Birkmayer W; Hornykiewicz O The L-3,4-dioxyphenylalanine (DOPA)-effect in Parkinson-akinesia. Wien. Klin. Wochenschr 1961, 73, 787–788. [PubMed: 13869404]

(24). Hornykiewicz O L-DOPA: From a Biologically Inactive Amino Acid to a Successful Therapeutic Agent. Amino Acids 2002, 23 (1–3), 65–70. [PubMed: 12373520]

(25). Tambasco N; Romoli M; Calabresi P Levodopa in Parkinson’s Disease: Current Status and Future Developments. Curr. Neuropharmacol 2018, 16 (8), 1239–1252. [PubMed: 28494719]

(26). Thomas TC; Kruzich PJ; Joyce BM; Gash CR; Suchland K; Surgener SP; Rutherford EC; Grandy DK; Gerhardt GA; Glaser PEA Dopamine D4 Receptor Knockout Mice Exhibit Neurochemical Changes Consistent with Decreased Dopamine Release. J. Neurosci. Methods 2007, 166 (2), 306–314. [PubMed: 17449106]

(27). Friedman NP; Robbins TW The Role of Prefrontal Cortex in Cognitive Control and Executive Function. Neuropsychopharmacology 2022, 47 (1), 72–89. [PubMed: 34408280]

(28). Rajmohan V; Mohandas E The Limbic System. Indian J. Psychiatry 2007, 49 (2), 132–139. [PubMed: 20711399]

(29). O’Malley KL; Harmon S; Tang L; Todd RD The Rat Dopamine D4 Receptor: Sequence, Gene Structure, and Demonstration of Expression in the Cardiovascular System. New Biol 1992, 4 (2), 137–146. [PubMed: 1554689]

(30). Van Tol HHM; Bunzow JR; Guan H-C; Sunahara RK; Seeman P; Niznik HB; Civelli O Cloning of the Gene for a Human Dopamine D4 Receptor with High Affinity for the Antipsychotic Clozapine. Nature 1991, 350 (6319), 610–614. [PubMed: 1840645]

(31). Cohen AI; Todd RD; Harmon S; O’Malley KL Photoreceptors of Mouse Retinas Possess D4 Receptors Coupled to Adenylate Cyclase. Proc. Natl. Acad. Sci. U.S.A 1992, 89 (24), 12093–12097. [PubMed: 1334557]

(32). Matsumoto M; Hidaka K; Tada S; Tasaki Y; Yamaguchi T Full-Length cDNA Cloning and Distribution of Human Dopamine D4 Receptor. Mol. Brain Res 1995, 29 (1), 157–162. [PubMed: 7769992]

(33). Mrzljak L; Bergson C; Pappy M; Huff R; Levenson R; Goldman-Rakic PS Localization of Dopamine D4 Receptors in GABAergic Neurons of the Primate Brain. Nature 1996, 381 (6579), 245–248. [PubMed: 8622768]

(34). Ariano MA; Wang J; Noblett KL; Larson ER; Sibley DR Cellular Distribution of the Rat D4 Dopamine Receptor Protein in the CNS Using Anti-Receptor Antisera. Brain Res 1997, 752 (1–2), 26–34. [PubMed: 9106437]

(35). Ptacek R; Kuzelova H; Stefano GB Dopamine D4 Receptor Gene DRD4 and Its Association with Psychiatric Disorders. Med. Sci. Monit 2011, 17 (9), RA215–RA220. [PubMed: 21873960]

(36). Defagot MC; Falzone TL; Low MJ; Grandy DK; Rubinstein M; Antonelli MC Quantitative Analysis of the Dopamine D4 Receptor in the Mouse Brain. J. Neurosci. Res 2000, 59 (2), 202–208. [PubMed: 10650878]

(37). Meador-Woodruff JH Dopamine Receptor Transcript Expression in Striatum and Prefrontal and Occipital Cortex: Focal Abnormalities in Orbitofrontal Cortex in Schizophrenia. Arch. Gen. Psychiatry 1997, 54 (12), 1089. [PubMed: 9400344]

(38). Lidow MS; Wang F; Cao Y; Goldman-Rakic PS Layer V Neurons Bear the Majority of mRNAs Encoding the Five Distinct Dopamine Receptor Subtypes in the Primate Prefrontal Cortex. Synapse 1998, 28 (1), 10–20. [PubMed: 9414013]

(39). Primus RJ; Thurkauf A; Xu J; Yevich E; McInerney S; Shaw K; Tallman JF; Gallagher DW II. Localization and Characterization of Dopamine D4 Binding Sites in Rat and Human Brain by Use of the Novel, D4 Receptor-Selective Ligand [3H]NGD 94–1. J. Pharmacol. Exp. Ther 1997, 282 (2), 1020–1027. [PubMed: 9262371]

(40). Meador-Woodruff JH; Grandy DK; Van Tol HHM; Damask SP; Little KY; Civelli O; Watson SJ Dopamine Receptor Gene Expression in the Human Medial Temporal Lobe. Neuropsychopharmacology 1994, 10 (4), 239–248. [PubMed: 7945734]

(41). Di Ciano P; Grandy DK; Le Foll B Dopamine D4 Receptors in Psychostimulant Addiction. Advances in Pharmacology; Elsevier, 2014; Vol. 69, pp 301–321.. [PubMed: 24484981]

(42). Gornick MC; Addington A; Shaw P; Bobb AJ; Sharp W; Greenstein D; Arepalli S; Castellanos FX; Rapoport JL Association of the Dopamine Receptor D4 (DRD4) Gene 7-repeat Allele with Children with Attention-deficit/Hyperactivity Disorder (ADHD): An Update. Am. J. Med. Genet., Part B 2007, 144B (3), 379–382. [PubMed: 17171657]

(43). Zhang K; Davids E; Tarazi F; Baldessarini R Effects of Dopamine D4 Receptor-Selective Antagonists on Motor Hyperactivity in Rats with Neonatal 6-Hydroxydopamine Lesions. Psychopharmacology 2002, 161 (1), 100–106. [PubMed: 11967637]

(44). Avale ME; Falzone TL; Gelman DM; Low MJ; Grandy DK; Rubinstein M The Dopamine D4 Receptor Is Essential for Hyperactivity and Impaired Behavioral Inhibition in a Mouse Model of Attention Deficit/Hyperactivity Disorder. Mol. Psychiatry 2004, 9 (7), 718–726. [PubMed: 14699433]

(45). Huot P; Johnston TH; Koprich JB; Aman A; Fox SH; Brotchie JM L-745,870 Reduces L-DOPA-Induced Dyskinesia in the 1-Methyl-4-Phenyl-1,2,3,6-Tetrahydropyridine-Lesioned Macaque Model of Parkinson’s Disease. J. Pharmacol. Exp. Ther 2012, 342 (2), 576–585. [PubMed: 22619253]

(46). Erlij D; Acosta-García J; Rojas-Márquez M; González-Hernández B; Escartín-Perez E; Aceves J; Florán B Dopamine D4 Receptor Stimulation in GABAergic Projections of the Globus Pallidus to the Reticular Thalamic Nucleus and the Substantia Nigra Reticulata of the Rat Decreases Locomotor Activity. Neuropharmacology 2012, 62 (2), 1111–1118. [PubMed: 22108379]

(47). Bastide MF; Meissner WG; Picconi B; Fasano S; Fernagut P-O; Feyder M; Francardo V; Alcacer C; Ding Y; Brambilla R; Fisone G; Jon Stoessl A; Bourdenx M; Engeln M; Navailles S; De Deurwaerdère P; Ko WKD; Simola N; Morelli M; Groc L; Rodriguez M-C; Gurevich EV; Quik M; Morari M; Mellone M; Gardoni F; Tronci E; Guehl D; Tison F; Crossman AR; Kang UJ; Steece-Collier K; Fox S; Carta M; Angela Cenci M; Bézard E Pathophysiology of L-Dopa-Induced Motor and Non-Motor Complications in Parkinson’s Disease. Prog. Neurobiol 2015, 132, 96–168. [PubMed: 26209473]

(48). Conde Rojas I; Acosta-García J; Caballero-Florán RN; Jijón-Lorenzo R; Recillas-Morales S; Avalos-Fuentes JA; Paz-Bermúdez F; Leyva-Gómez G; Cortés H; Florán B Dopamine D4 Receptor Modulates Inhibitory Transmission in Pallido-pallidal Terminals and Regulates Motor Behavior. Eur. J. Neurosci 2020, 52 (11), 4563–4585. [PubMed: 33098606]

(49). Coward DM General Pharmacology of Clozapine. Br. J. Psychiatry 1992, 160 (S17), 5–11.

(50). Patel S; Freedman S; Chapman KL; Emms F; Fletcher AE; Knowles M; Marwood R; Mcallister G; Myers J; Curtis N; Kulagowski JJ; Leeson PD; Ridgill M; Graham M; Matheson S; Rathbone D; Watt AP; Bristow LJ; Rupniak NM; Baskin E; Lynch JJ; Ragan CI Biological Profile of L-745,870, a Selective Antagonist with High Affinity for the Dopamine D4 Receptor. J. Pharmacol. Exp. Ther 1997, 283 (2), 636–647. [PubMed: 9353380]

(51). Kramer MS The Effects of a Selective D4 Dopamine Receptor Antagonist (L-745,870) in Acutely Psychotic Inpatients With Schizophrenia. Arch. Gen. Psychiatry 1997, 54 (6), 567. [PubMed: 9193198]

(52). Bristow LJ; Collinson N; Cook GP; Curtis N; Freedman SB; Kulagowski JJ; Leeson PD; Patel S; Ragan CI; Ridgill M; Saywell KL; Tricklebank MD L-745,870, a Subtype Selective Dopamine D4 Receptor Antagonist, Does Not Exhibit a Neuroleptic-like Profile in Rodent Behavioral Tests. J. Pharmacol. Exp. Ther 1997, 283 (3), 1256–1263. [PubMed: 9400001]

(53). Janssen PAJ; Jageneau AHM; Schellekens KHL Chemistry and Pharmacology of Compounds Related to 4-(4-Hydroxy-4-Phenyl-Piperidino)-Butyrophenone: Part IV Influence of Haloperidol (R 1625) and of Chlorpromazine on the Behaviour of Rats in an Unfamiliar “Open Field” Situation. Psychopharmacologia 1960, 1 (5), 389–392. [PubMed: 13789498]

(54). Divry P; Bobon J; Collard J; Pinchard A; Nols E Study & clinical trial of R 1625 or haloperidol, a new neuroleptic & so-called neurodysleptic agent. Acta Neurol. Psychiatr. Belg 1959, 59 (3), 337–366. [PubMed: 13649275]

(55). Janssen PAJ; Van De Westeringh C.; Jageneau AHM; Demoen PJA; Hermans BKF; Van Daele GHP; Schellekens KHL; Van Der Eycken CAM; Niemegeers CJE Chemistry and Pharmacology of CNS Depressants Related to 4-(4-Hydroxy-4-Phenylpiperidino)Butyrophenone Part I-Synthesis and Screening Data in Mice. J. Med. Pharm. Chem 1959, 1 (3), 281–297. [PubMed: 14406750]

(56). Divry P; Bobon J; Collard J [R-1625: a new drug for the symptomatic treatment of psychomotor excitation]. Acta Neurol. Psychiatr. Belg 1958, 58 (10), 878–888. [PubMed: 13605678]

(57). Sanner MA; Chappie TA; Dunaiskis AR; Fliri AF; Desai KA; Zorn SH; Jackson ER; Johnson CG; Morrone JM; Seymour PA; Majchrzak MJ; Stephen Faraci W; Collins JL; Duignan DB; Di Prete CC; Lee JS; Trozzi A Synthesis, Sar and Pharmacology of CP-293,019: A Potent, Selective Dopamine D4 Receptor Antagonist. Bioorg. Med. Chem. Lett 1998, 8 (7), 725–730. [PubMed: 9871530]

(58). Witt JO; McCollum AL; Hurtado MA; Huseman ED; Jeffries DE; Temple KJ; Plumley HC; Blobaum AL; Lindsley CW; Hopkins CR Synthesis and Characterization of a Series of Chiral Alkoxymethyl Morpholine Analogs as Dopamine Receptor 4 (D4R) Antagonists. Bioorg. Med. Chem. Lett 2016, 26 (10), 2481–2488. [PubMed: 27080176]

(59). Tolentino KT; Mashinson V; Vadukoot AK; Hopkins CR Discovery and Characterization of Benzyloxy Piperidine Based Dopamine 4 Receptor Antagonists. Bioorg. Med. Chem. Lett 2022, 61, 128615. [PubMed: 35151866]

(60). Ford B; Lynch T; Greene P Risperidone in Parkinson’s Disease. Lancet 1994, 344 (8923), 681.

(61). Friedman JH; Berman RM; Goetz CG; Factor SA; Ondo WG; Wojcieszek J; Carson WH; Marcus RN Open-label Flexible-dose Pilot Study to Evaluate the Safety and Tolerability of Aripiprazole in Patients with Psychosis Associated with Parkinson’s Disease. Mov. Disord 2006, 21 (12), 2078–2081. [PubMed: 17013906]

(62). Kurtz AL; Kaufer DI Dementia in Parkinson’s Disease. Curr. Treat. Options Neurol 2011, 13 (3), 242–254. [PubMed: 21461668]

(63). Aubert I; Guigoni C; Håkansson K; Li Q; Dovero S; Barthe N; Bioulac BH; Gross CE; Fisone G; Bloch B; Bezard E Increased D_1 Dopamine Receptor Signaling in Levodopa-induced Dyskinesia. Ann. Neurol 2005, 57 (1), 17–26. [PubMed: 15514976]

(64). Darmopil S; Martín AB; De Diego IR; Ares S; Moratalla R Genetic Inactivation of Dopamine D1 but Not D2 Receptors Inhibits L-DOPA-Induced Dyskinesia and Histone Activation. Biol. Psychiatr 2009, 66 (6), 603–613.

(65). Jeffries DE; Witt JO; McCollum AL; Temple KJ; Hurtado MA; Harp JM; Blobaum AL; Lindsley CW; Hopkins CR Discovery, Characterization and Biological Evaluation of a Novel (R)-4,4-Difluoropiperidine Scaffold as Dopamine Receptor 4 (D 4 R) Antagonists. Bioorg. Med. Chem. Lett 2016, 26 (23), 5757–5764. [PubMed: 28327307]

(66). Berry CB; Bubser M; Jones CK; Hayes JP; Wepy JA; Locuson CW; Daniels JS; Lindsley CW; Hopkins CR Discovery and Characterization of ML398, a Potent and Selective Antagonist of the D_4 Receptor with *in Vivo* Activity. ACS Med. Chem. Lett 2014, 5 (9), 1060–1064. [PubMed: 25221667]

(67). Boateng CA; Nilson AN; Placide R; Pham ML; Jakobs FM; Boldizsar N; McIntosh S; Stallings LS; Korankyi IV; Kelshikar S; Shah N; Panasis D; Muccilli A; Ladik M; Maslonka B; McBride C; Sanchez MX; Akca E; Alkhatib M; Saez J; Nguyen C; Kurtyan E; DePierro J; Crowthers R; Brunt D; Bonifazi A; Newman AH; Rais R; Slusher BS; Free RB; Sibley DR; Stewart KD; Wu C; Hemby SE; Keck TM Pharmacology and Therapeutic Potential of Benzothiazole Analogues for Cocaine Use Disorder. J. Med. Chem 2023, 66 (17), 12141–12162. [PubMed: 37646374]

(68). Zhou Y; Cao C; He L; Wang X; Zhang XC Crystal Structure of Dopamine Receptor D4 Bound to the Subtype Selective Ligand, L745870. eLife 2019, 8, No. e48822. [PubMed: 31750832]

(69). Wang S; Wacker D; Levit A; Che T; Betz RM; McCorvy JD; Venkatakrishnan AJ; Huang X-P; Dror RO; Shoichet BK; Roth BL D_4 Dopamine Receptor High-Resolution Structures Enable the Discovery of Selective Agonists. Science 2017, 358 (6361), 381–386. [PubMed: 29051383]

(70). Brown BP; Mendenhall J; Meiler J BCL::MolAlign: Three-Dimensional Small Molecule Alignment for Pharmacophore Mapping. J. Chem. Inf. Model 2019, 59 (2), 689–701. [PubMed: 30707580]

(71). Carato P; Graulich A; Jensen N; Roth BL; Liégeois JF Synthesis and in Vitro Binding Studies of Substituted Piperidine Naphthamides. Part II: Influence of the Substitution on the Benzyl Moiety on the Affinity for D2L, D4.2, and 5-HT2A Receptors. Bioorg. Med. Chem. Lett 2007, 17 (6), 1570–1574. [PubMed: 17251022]

(72). Chai J-D; Head-Gordon M Long-Range Corrected Hybrid Density Functionals with Damped Atom-Atom Dispersion Corrections. Phys. Chem. Chem. Phys 2008, 10 (44), 6615. [PubMed: 18989472]

(73). Gaus M; Cui Q; Elstner M DFTB3: Extension of the SelfConsistent-Charge Density-Functional Tight-Binding Method (SCC-DFTB). J. Chem. Theory Comput 2011, 7 (4), 931–948.

(74). Brandenburg JG; Grimme S Accurate Modeling of Organic Molecular Crystals by Dispersion-Corrected Density Functional Tight Binding (DFTB). J. Phys. Chem. Lett 2014, 5 (11), 1785–1789. [PubMed: 26273854]

(75). Lovering F; Bikker J; Humblet C Escape from Flatland: Increasing Saturation as an Approach to Improving Clinical Success. J. Med. Chem 2009, 52 (21), 6752–6756. [PubMed: 19827778]

(76). Lovering F Escape from Flatland 2: Complexity and Promiscuity. MedChemComm 2013, 4 (3), 515.

(77). Talele TT Opportunities for Tapping into Three-Dimensional Chemical Space through a Quaternary Carbon. J. Med. Chem 2020, 63 (22), 13291–13315. [PubMed: 32805118]

(78). Hiesinger K; Dar'in D; Proschak E; Krasavin M Spirocyclic Scaffolds in Medicinal Chemistry. J. Med. Chem 2021, 64 (1), 150–183. [PubMed: 33381970]

(79). Tolentino KT; Mashinson V; Sharma MK; Chhonker YS; Murry DJ; Hopkins CR From Dopamine 4 to Sigma 1: Synthesis, SAR and Biological Characterization of a Piperidine Scaffold of Σ1 Modulators. Eur. J. Med. Chem 2022, 244, 114840. [PubMed: 36283180]

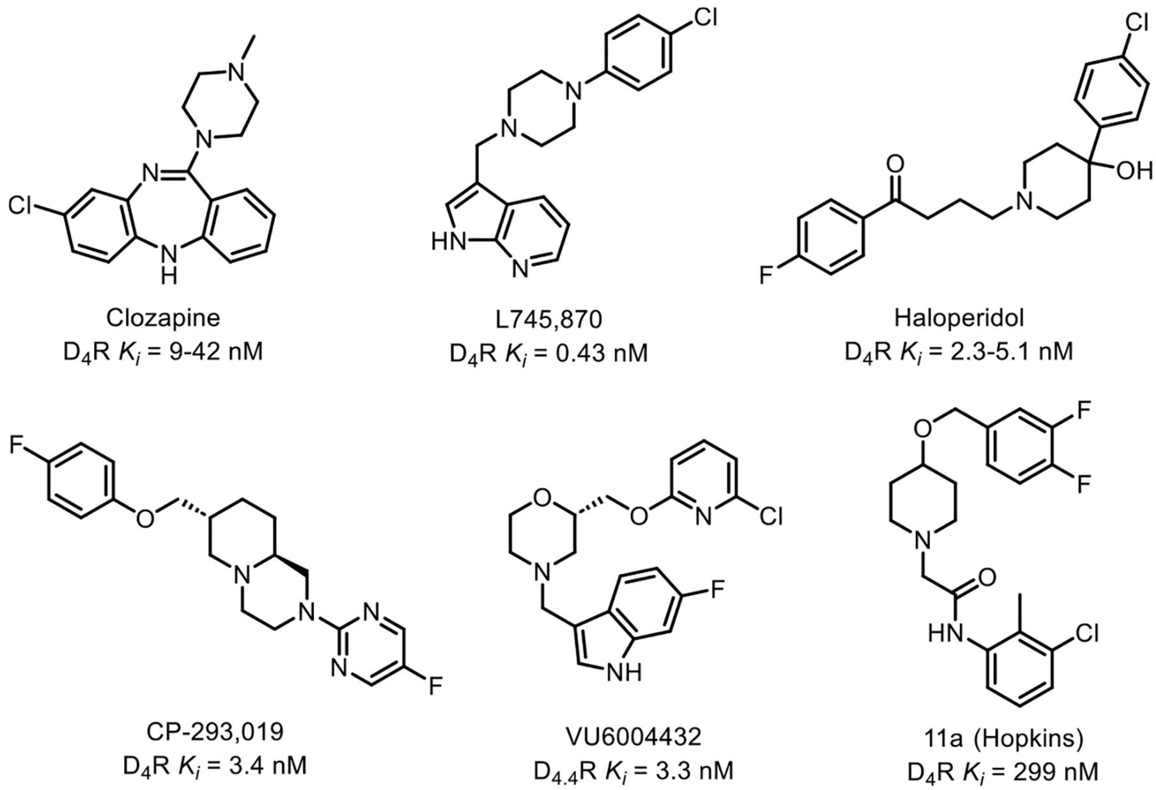

Figure 1.
Selected historical compounds demonstrating antagonism at D_4R.[9,30,49–59]

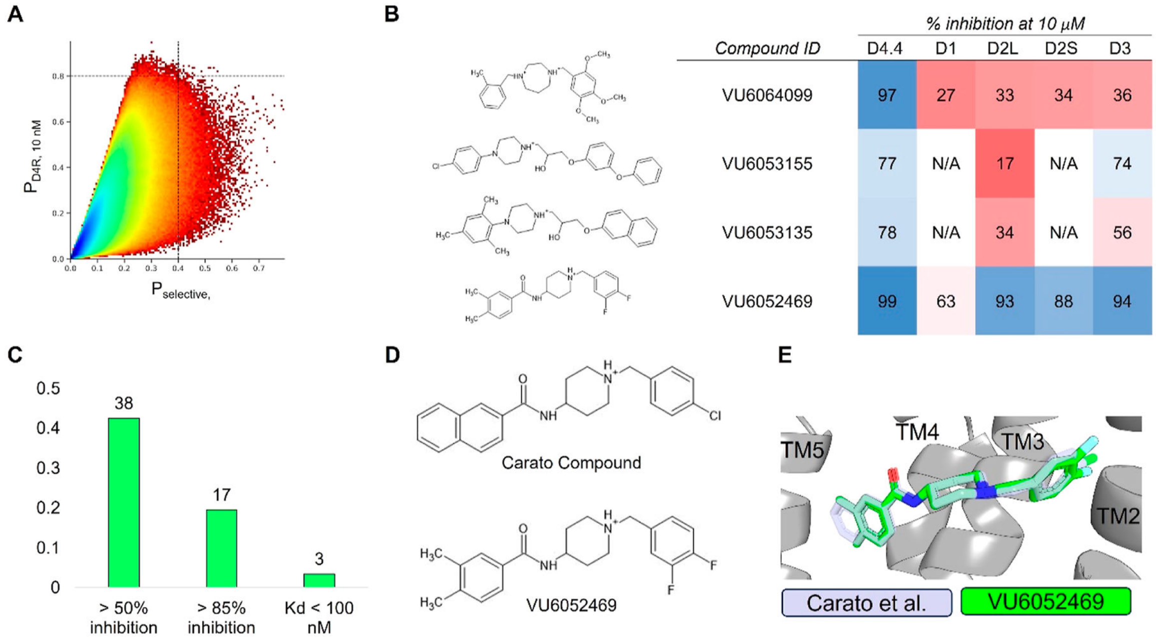

Figure 2.

Virtual high-throughput screening for D_4R antagonists. (A) Predicted D_4R activity vs selectivity from the ligand-based multitask ANN QSAR model ultralarge library virtual high-throughput screening. Dashed lines indicate QSAR-predicted active classification probabilities at or greater than 80% (horizontal) and 40% (vertical) for D_4R 10 nM activity and overall selectivity, respectively. Plot color is contoured by the density of molecules, with higher-density regions appearing blue and lower-density regions appearing red. (B) Sample molecules identified during the virtual high-throughput screening. (C) D_4R hit-rate for experimentally validated molecules. (D) 2D structures of Carato et al.: compound 22[71] and *VU6052469*. (E) Overlay of docked poses of Carato et al.: compound 22[71] and *VU6052469* within D_4R.

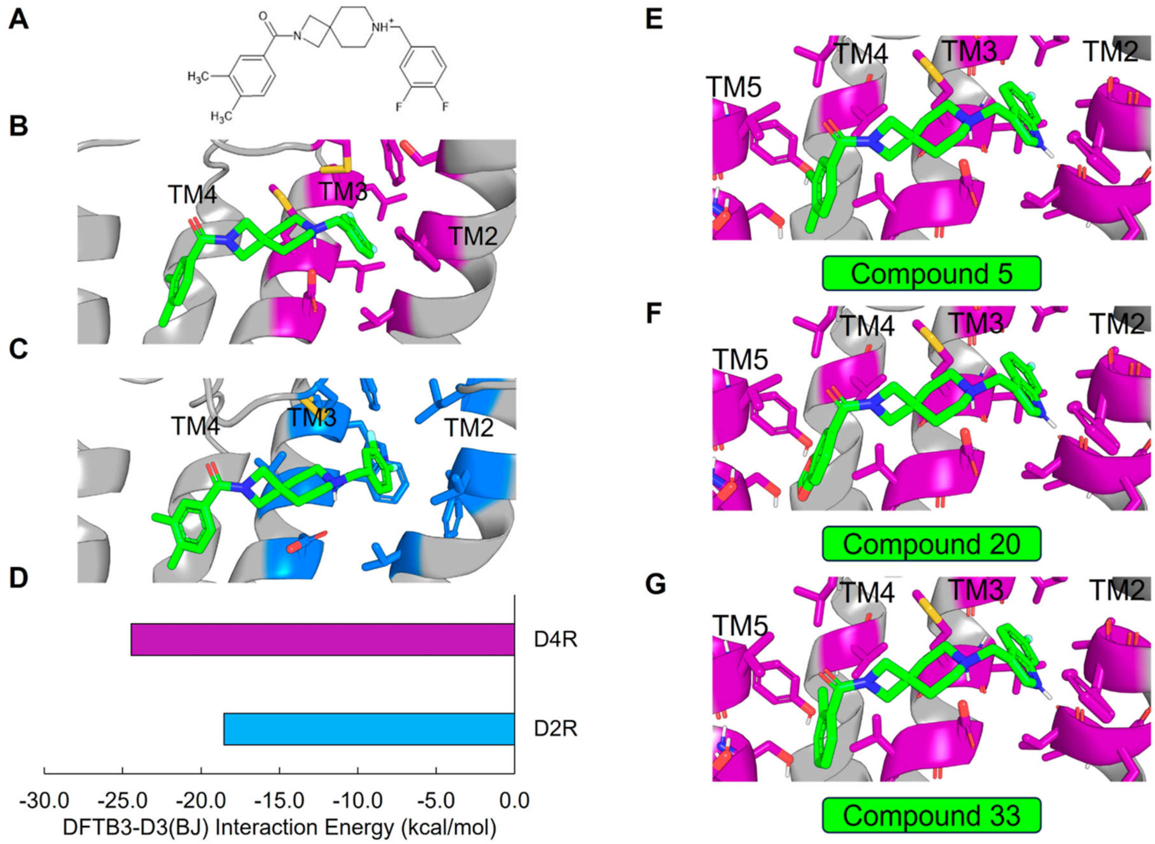

Figure 3.

SAR analysis of D_4R selective antagonists. (A) Chemical structure of the spirocyclic compound **4**. (B) Docked pose of compound **4** (green) in D_4R. (C) Docked pose of compound **4** (green) in D_2R. (D) DFTB3-D3(BJ) interaction energy (kcal/mol) between compound **4** and the central aspartate and TM2/TM3 hydrophobic pocket of D_4R (purple) and D_2R (blue). Docked poses of compounds (E) **5,** (F) **20,** and (G) **33.**

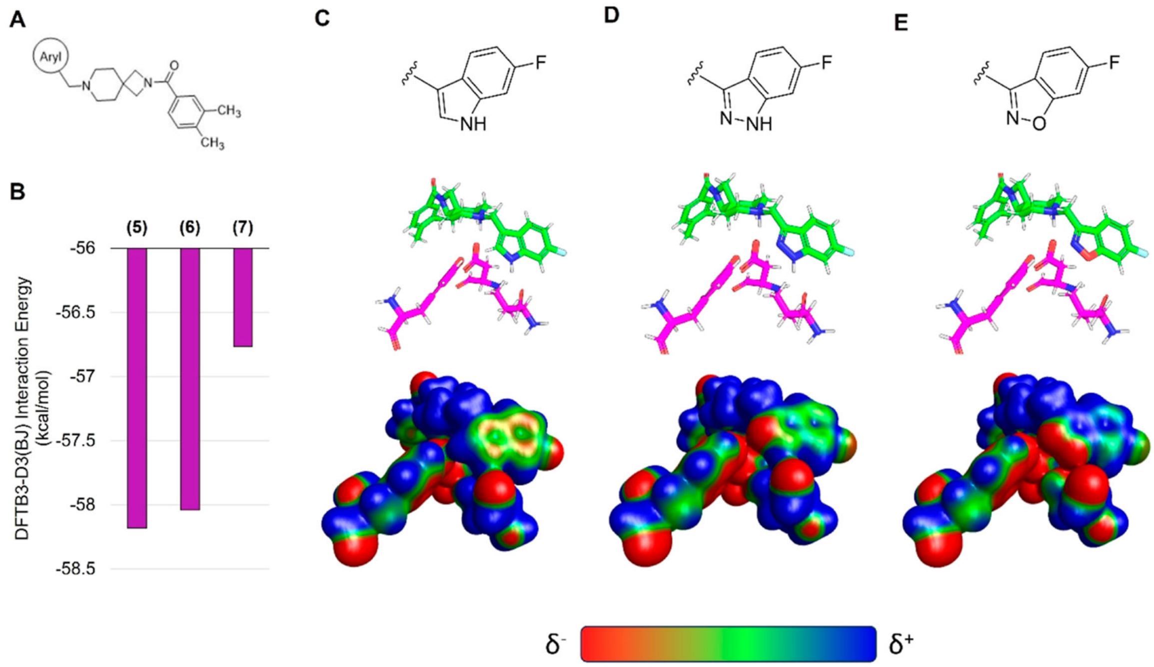

Figure 4.

Surface electrostatics analysis of D_4R selective antagonists in complex with D_4R. (A) Schematic southern aryl substitution on compound **4.** (B) Interaction energies for the model systems containing compounds **5, 6,** or **7.** Surface electrostatic potential analysis of (C) compound **5,** (D) compound 6, and (E) compound **7.** Electrostatic potentials are calculated for model systems (C–D) at the wB97X-D/6–31G(d) level of theory with solvation model density (SMD) aqueous implicit solvent following geometry optimization of the receptor pocket and ligand in complex utilizing DFTB3-D3(BJ) with SMD solvent water.

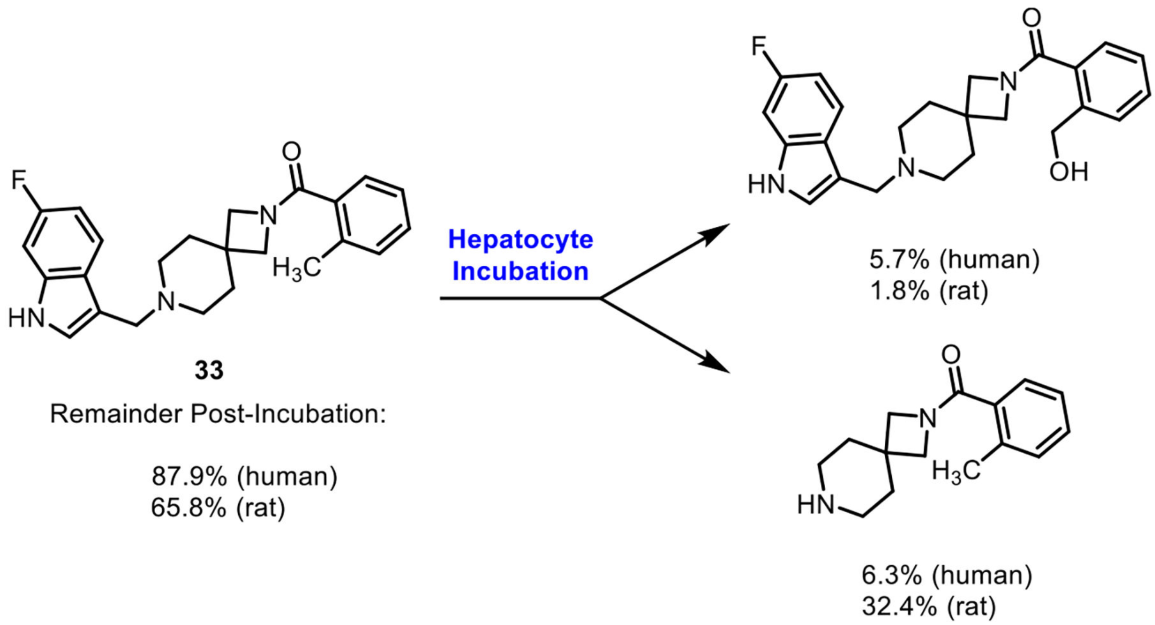

Figure 5.

Metabolite analysis of compound **33** in human and rat hepatocytes. Parent compound incubated in human or rat hepatocytes for **4** h. Percentages (determined via LC/MS) indicate the relative percentage of compounds present postincubation. See Supporting Information for details.

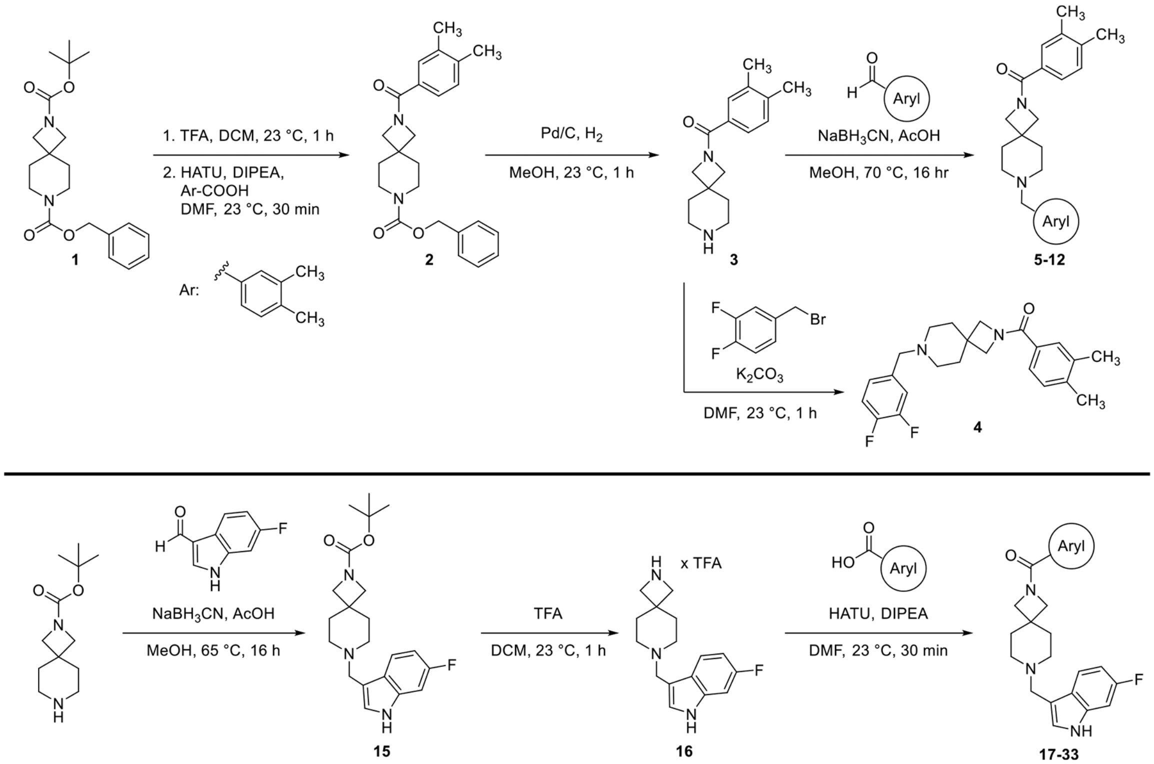

Scheme 1.

Synthesis of Diazaspiro[3.5]nonane D_4R Antagonists

Table 1.

Southern Region SAR

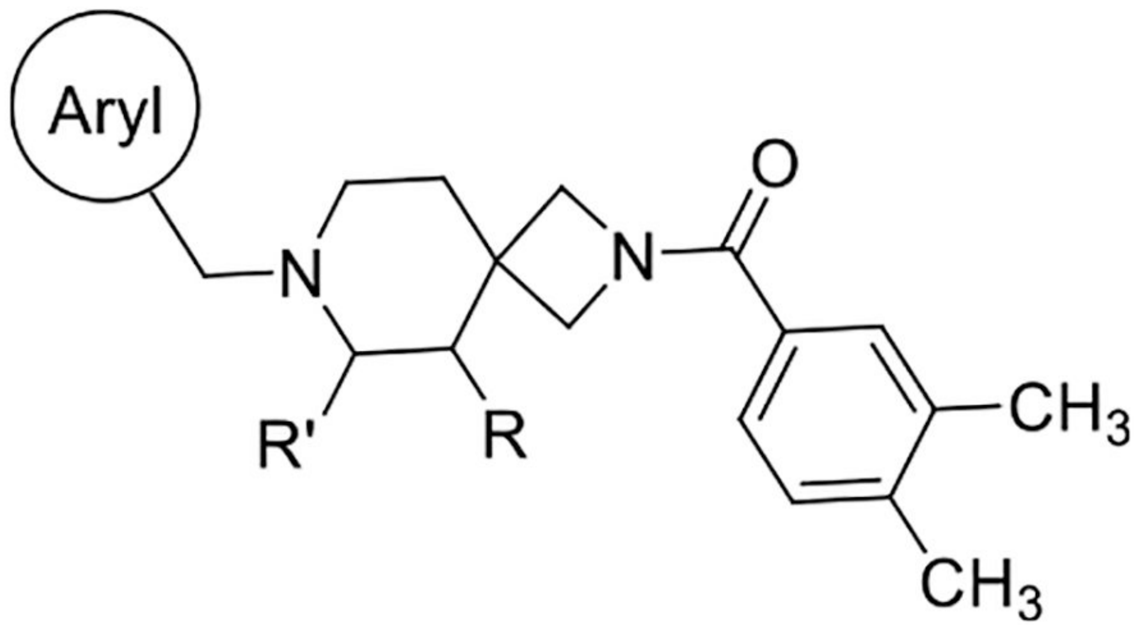

Cmpd No.	Aryl	R	R’	% Inhibition at 10 μM[a]					$D_{4.4}$ IC_{50} (nM)[a]	$D_{4.4}$ K_i(nM)[a]
				$D_{4.4}$	D_{2S}	D_{2L}	D_3	D_1		
4	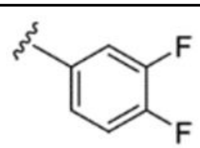	H	H	88%	8%	9%	9%	21%	2790	250
5	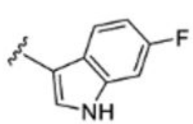	H	H	94%	25%	24%	27%	35%	200	56

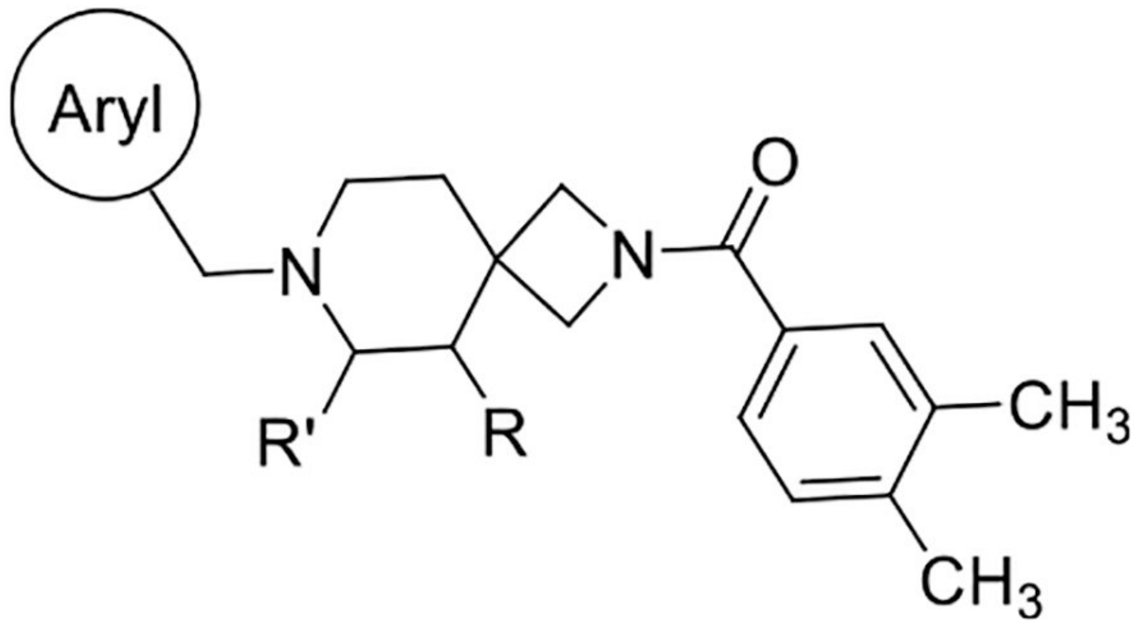

Cmpd No.	Aryl	R	R'	% Inhibition at 10 μM[a]					$D_{4.4}$ IC_{50} (nM)[a]	$D_{4.4}$ K_i(nM)[a]
				$D_{4.4}$	D_{2S}	D_{2L}	D_3	D_1		
6	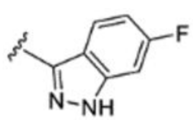	H	H	90%	15%	3%	25%	−4%	150	43
7	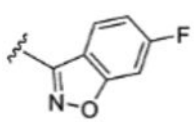	H	H	20%	-	-	-	-	-	-

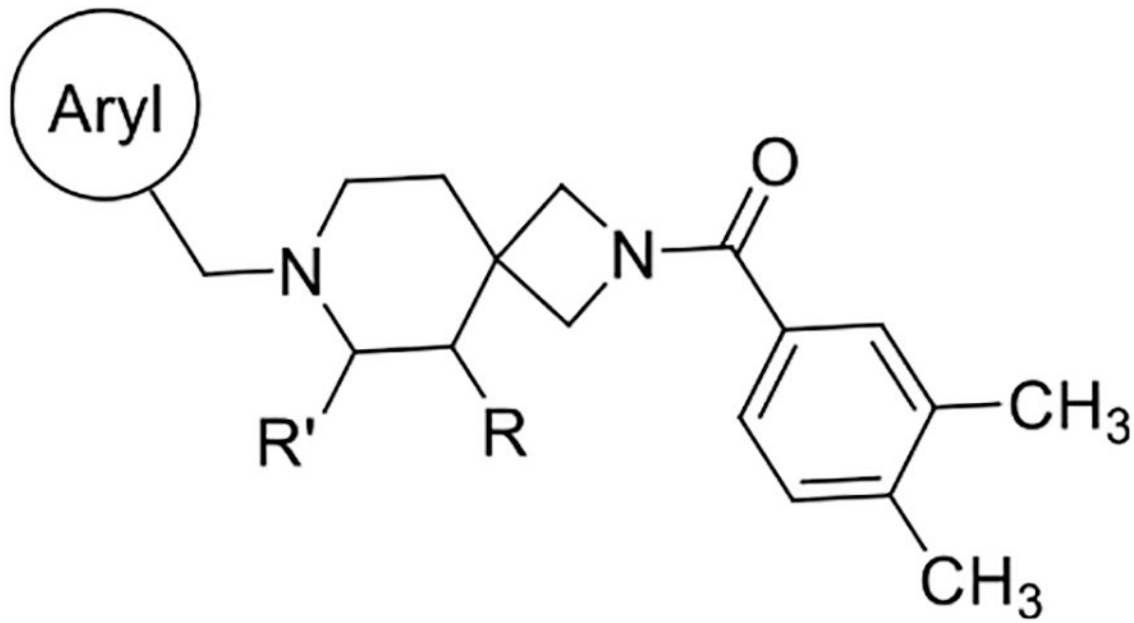

Cmpd No.	Aryl	R	R’	% Inhibition at 10 μM[a]					$D_{4.4}$ IC_{50} (nM)[a]	$D_{4.4}$ K_i(nM)[a]
				$D_{4.4}$	D_{2S}	D_{2L}	D_3	D_1		
8	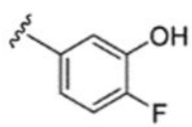	H	H	62%	-	-	-	-	-	-
9	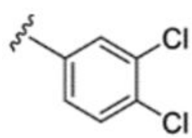	H	H	91%	25%	24%	62%	24%	81	22

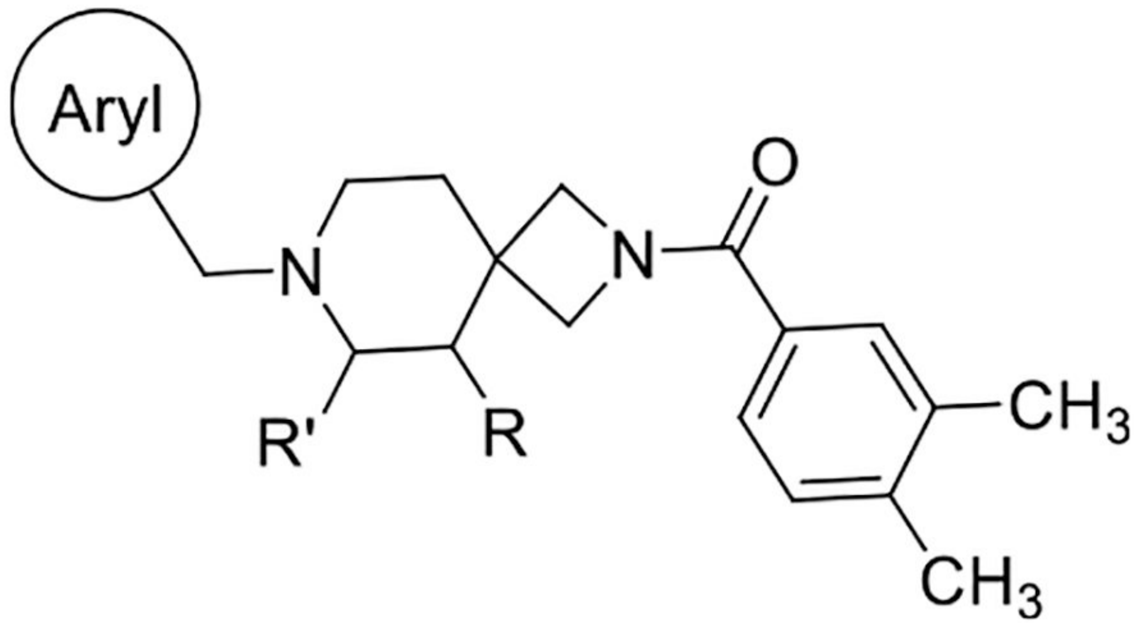

Cmpd No.	Aryl	R	R'	% Inhibition at 10 μM[a]					$D_{4.4}$ IC_{50} (nM)[a]	$D_{4.4}$ K_i(nM)[a]
				$D_{4.4}$	D_{2S}	D_{2L}	D_3	D_1		
10	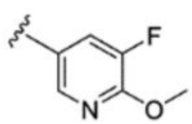	H	H	66%	-	-	-	-	-	-
11	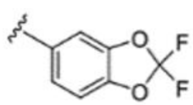	H	H	66%	-	-	-	-	-	-

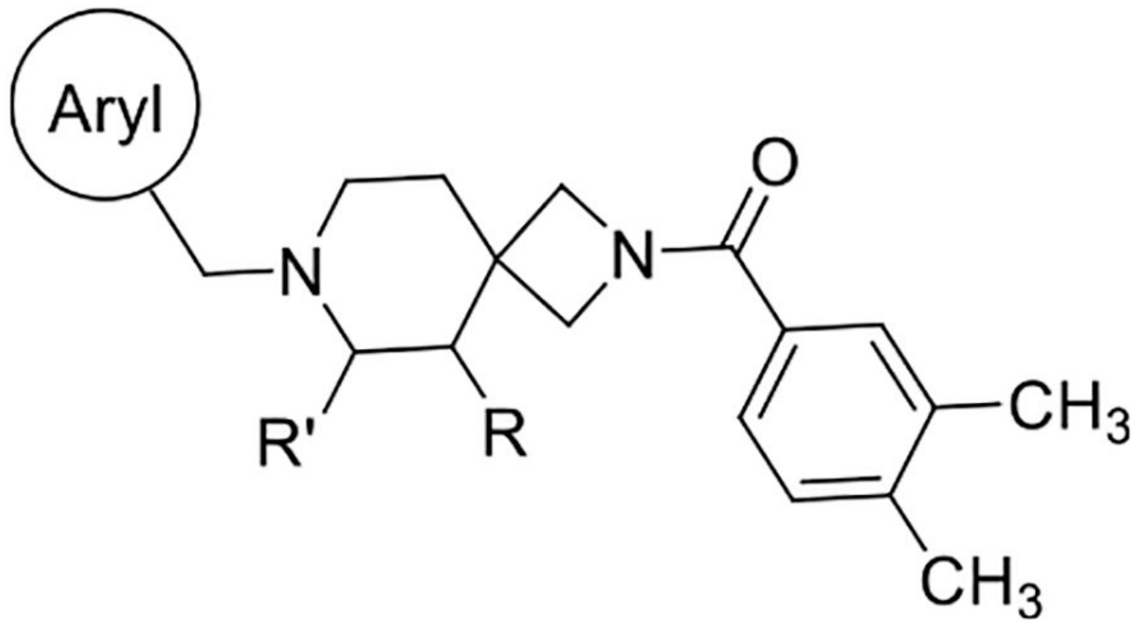

Cmpd No.	Aryl	R	R’	% Inhibition at 10 μM[a]					$D_{4.4}$ IC_{50} (nM)[a]	$D_{4.4}$ K_i(nM)[a]
				$D_{4.4}$	D_{2S}	D_{2L}	D_3	D_1		
12	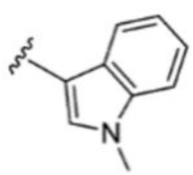	H	H	92%	24%	16%	19%	27%	280	76
13	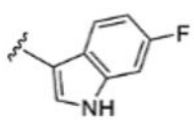	CH_3	H	85%	-	-	-	-	990	270

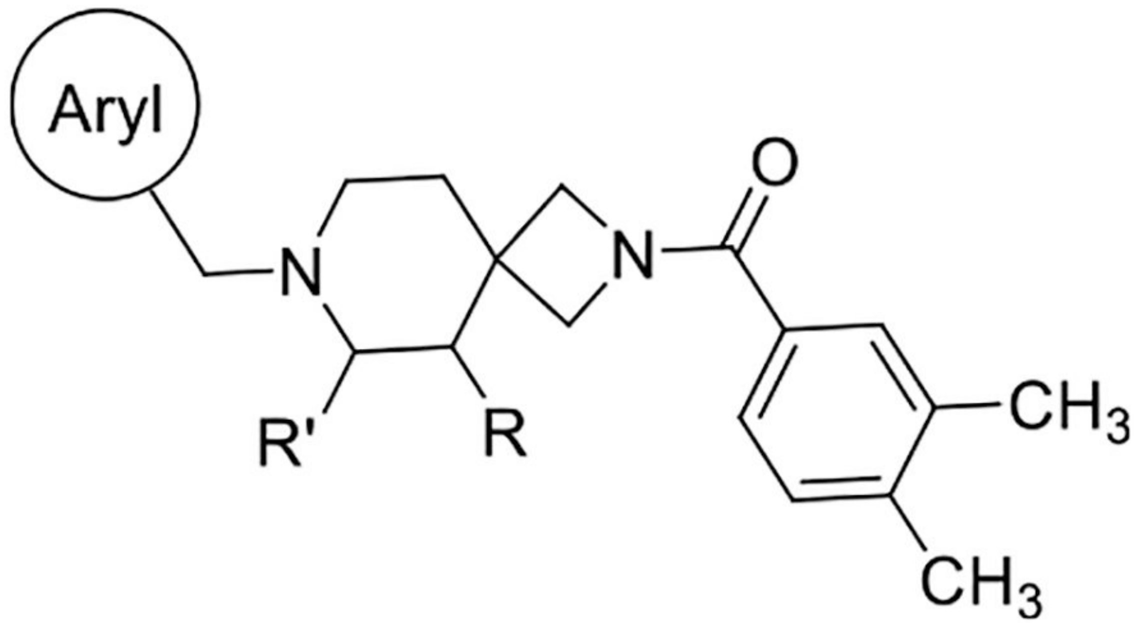

Cmpd No.	Aryl	R	R'	% Inhibition at 10 μM[a]					$D_{4.4}$ IC_{50} (nM)[a]	$D_{4.4}$ K_i(nM)[a]
				$D_{4.4}$	D_{2S}	D_{2L}	D_3	D_1		
14	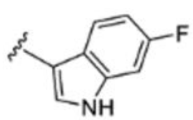	H	CH_3	89%	-	-	-	-	1920	530

[a]Values were obtained from Eurofins Discovery. See Supporting Information for more details.

Table 2.

Northern Ring SAR

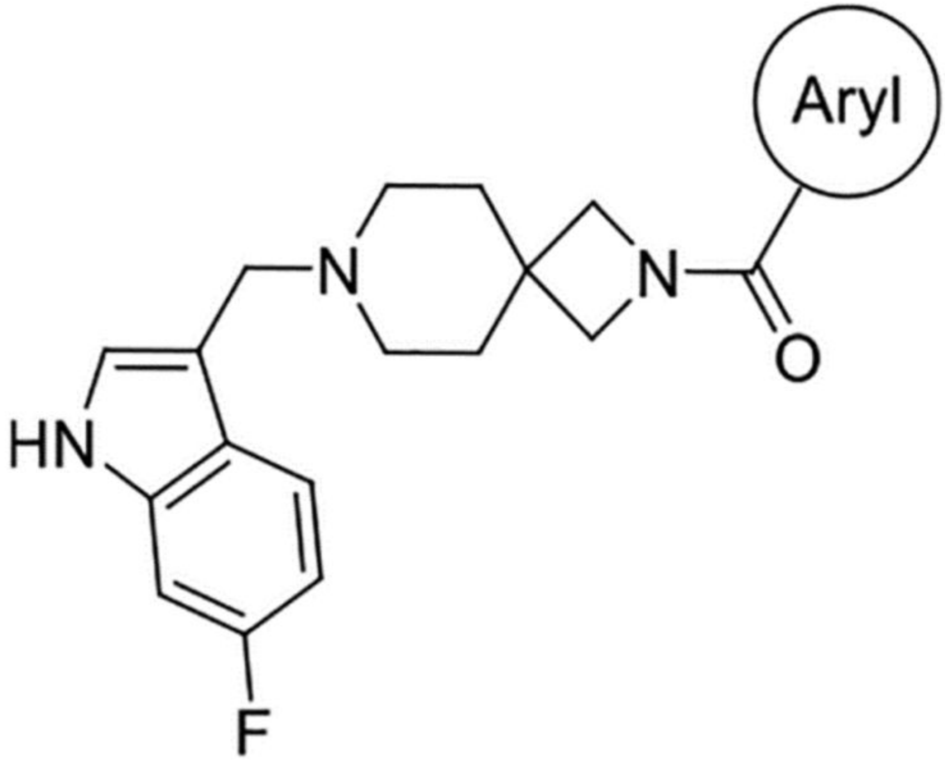

Cmpd No.	Aryl	% Inhibition at 10 µM[b]					$D_{4.4}$ IC_{50} (nM)[a]	$D_{4.}$ K_i(nM
		$D_{4.4}$	D_{2S}	D_{2L}	D_3	D_1		
5	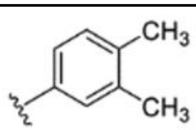	94%	25%	24%	27%	35%	200	56
17	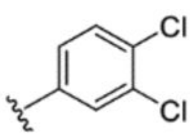	93%	11%	26%	34%	24%	77	21
18	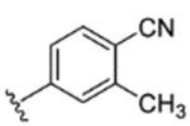	42%	-	-	-	-	-	-

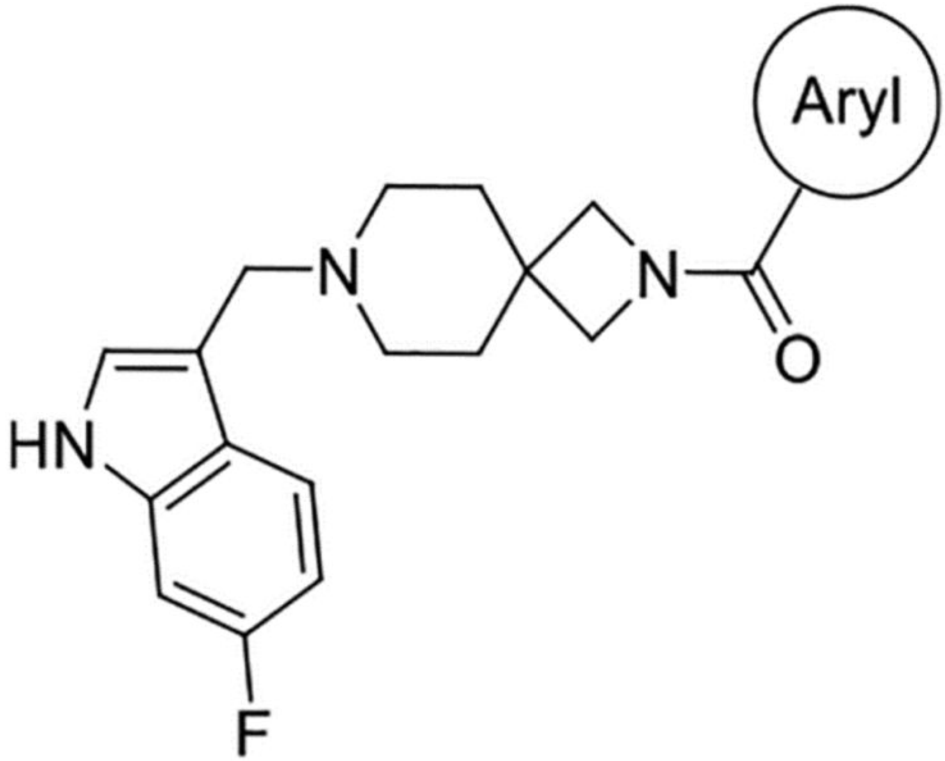

Cmpd No.	Aryl	% Inhibition at 10 μM[b]					$D_{4.4}$ IC_{50} (nM)[a]	$D_{4.}$ K_i(nM
		$D_{4.4}$	D_{2S}	D_{2L}	D_3	D_1		
19	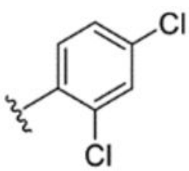	92%	14%	23%	30%	21%	82	23
20	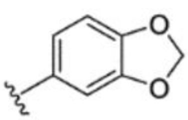	95%	12%	18%	14%	16%	84	23
21	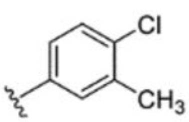	94%	17%	29%	40%	24%	78	22
22	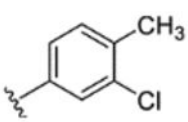	92%	22%	38%	31%	19%	95	26

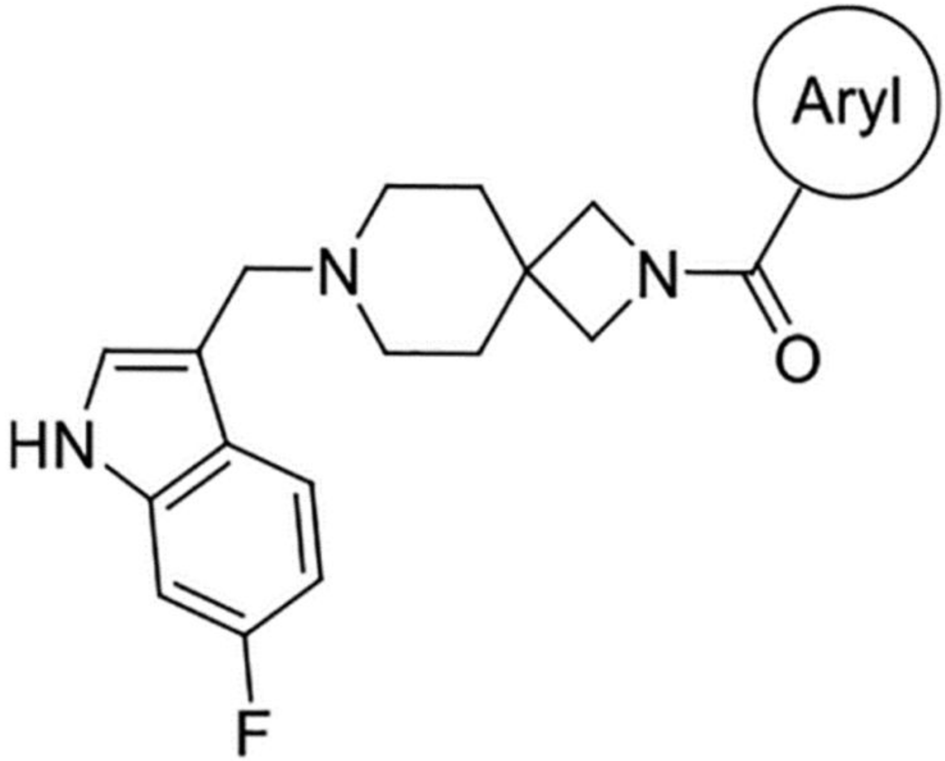

Cmpd No.	Aryl	% Inhibition at 10 μM[b]					$D_{4.4}$ IC_{50} (nM)[a]	D4. Ki(nM
		$D_{4.4}$	D_{2S}	D_{2L}	D_3	D_1		
23	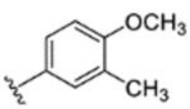	78%	-	-	-	-	-	-
24	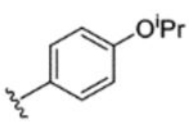	63%	-	-	-	-	-	-
25	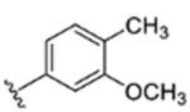	66%	-	-	-	-	-	-
26	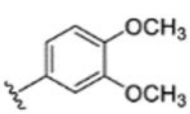	14%	-	-	-	-	-	-
27	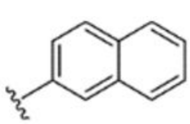	95%	21%	34%	36%	32%	28	7.6

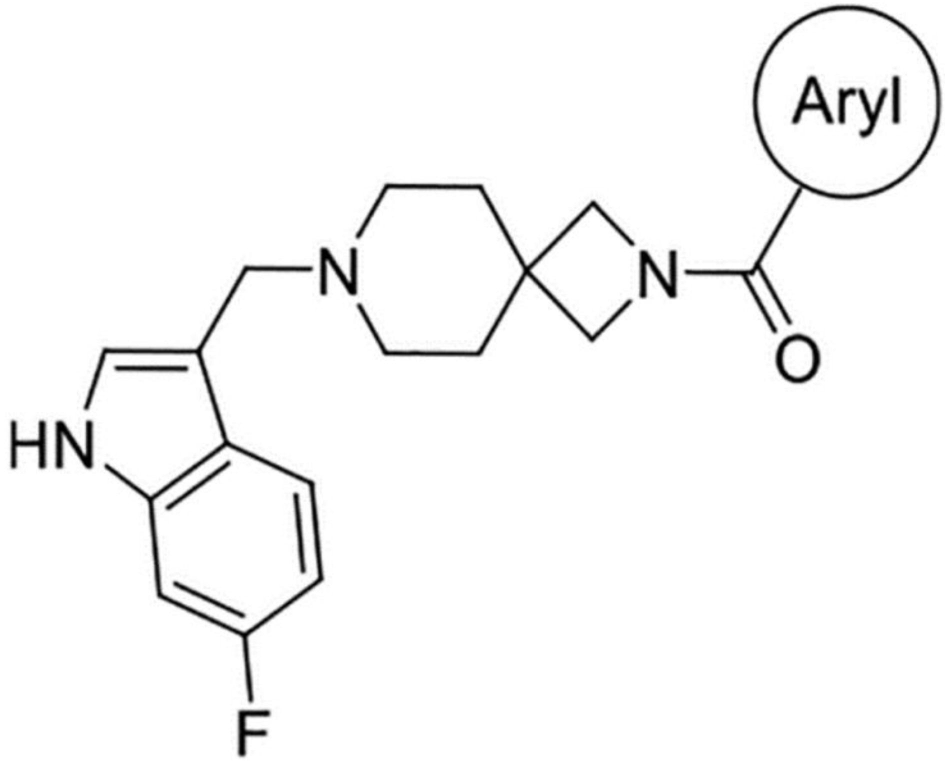

Cmpd No.	Aryl	% Inhibition at 10 μM[b]					D4.4 IC50 (nM)[a]	D4. Ki(nM
		$D_{4.4}$	D_{2S}	D_{2L}	D_3	D_1		
28	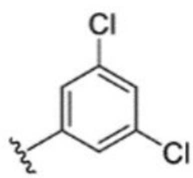	49%	-	-	-	-	-	-
29	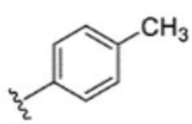	99%	5%	20%	13%	27%	62	17
30	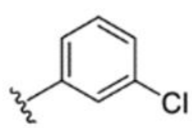	95%	17%	35%	23%	10%	790	220
31	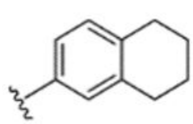	93%	22%	26%	35%	21%	260	71

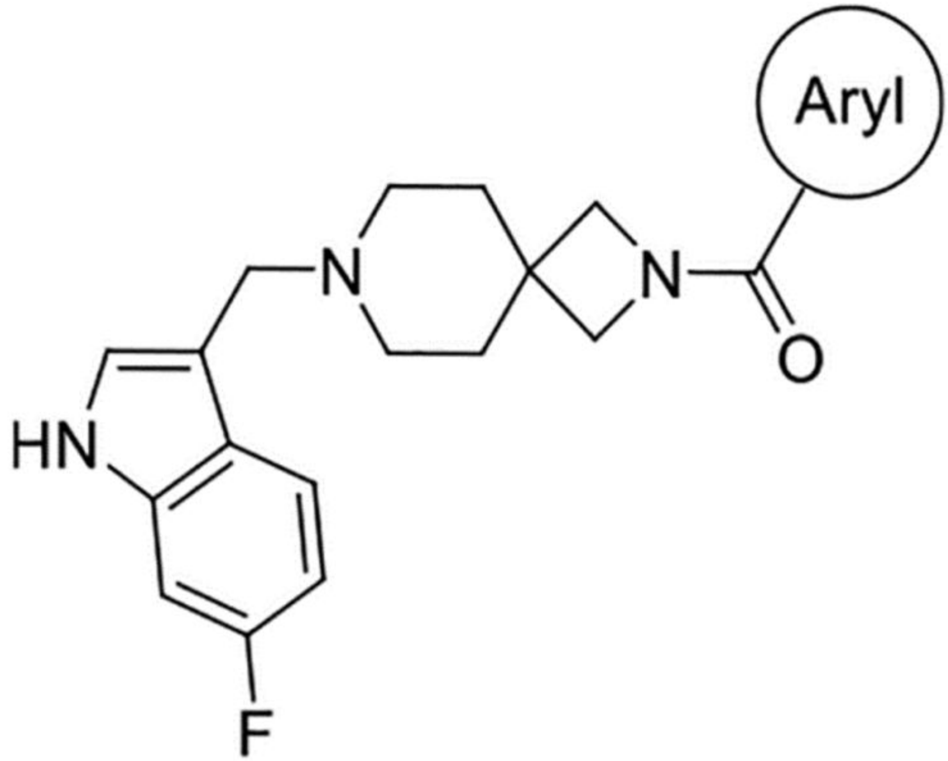

Cmpd No.	Aryl	% Inhibition at 10 μM[b]					$D_{4.4}$ IC_{50} (nM)[a]	$D_{4.}$ K_i(nM
		$D_{4.4}$	D_{2S}	D_{2L}	D_3	D_1		
32	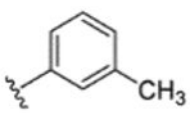	92%	18%	18%	12%	10%	490	14[illegible]
33	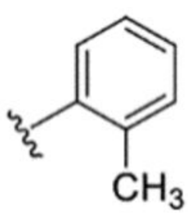	93%	0%	−7%	11%	9%	210	59
34[a]	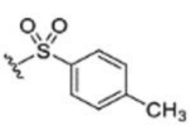	94%	17%	50%	49%	47%	120	33

[a]Structure for this compound is a sulfonamide bound to the azetidine nitrogen of the spirocycle.

[b]Values were obtained from Eurofins Discovery. See Supporting Information for more details.

Author Manuscript

Author Manuscript

Author Manuscript

Table 3.

In Vivo and In Vitro Results of Selected Compounds

compound	$f_{u,plasma}$ [a]		CL_H [a] (mL/min/kg)		CL_p [a] (mL/min/kg)	$t_{1/2}$ [a] (h)	V_{ss} [a] (L/kg)	AUC[a] (h·ng/mL)
	human	rat	human	rat				
4	0.01	0.03	16.9	59.1	116	1.05	5.52	28.7
33	0.19	0.26	16.0	39.0	123	4.02	36.9	27.0
32	0.06	0.14	14.7	46.2				
29	0.05	0.15	17.3	49.2				
20	0.10	0.23	13.7	36.2	126	4.55	44.4	26.4

[a] f_u = Fraction unbound; equilibrium dialysis assay; CL_H = hepatic clearance; CL_p = plasma clearance; $t_{1/2}$ = terminal phase plasma half-life; V_{ss} = volume of distribution at steady-state; AUC = area under the curve.